Characterization of the Daytime Ionosphere with ICON EUV Airglow Limb Profiles

Andrew W. Stephan[1] [ORCID] · Martin M. Sirk[2] · Eric J. Korpela[2] · Scott L. England[3] · Thomas J. Immel[2]

Abstract

The NASA Ionospheric Connection Explorer Extreme Ultraviolet spectrograph, ICON EUV, images one-dimensional altitude profiles of the daytime extreme-ultraviolet (EUV) airglow between 54-88 nm. This spectral range contains several OII emission features derived from the photoionization of atomic oxygen by solar EUV. The primary target of the ICON EUV is the bright OII (^4P – ^4S) triplet emission spanning 83.2-83.4 nm that is used in combination with a dimmer but complementary feature (^2P – ^2D) spanning 61.6-61.7 nm that are jointly analyzed with an algorithm that uses discrete inverse theory to optimize a forward model of these emissions to infer the best-fit solution of ionospheric O^+ density profile between 150-450 km. From this result, the daytime ionospheric F-region peak electron density and height, NmF2 and hmF2 respectively, are inferred. The science goals of ICON require these measurements be made in the regions of interest with a vertical resolution in hmF2 of 20 km and a 20% precision in NmF2 within a 60-second integration corresponding to a 500 km sampling along the orbit track. This paper describes the results from the ICON EUV over the first year of the mission, which occurred primarily under solar minimum conditions. It describes adjustments made to the algorithm to improve not only the quality of data products during this time, but also to improve speed and performance while simultaneously meeting the ICON measurement requirements. It also provides examples of results and an overview of key features and limitations to consider when using these products for scientific studies.

The Ionospheric Connection Explorer (ICON) Mission: First Results
Edited by David E. Siskind and Ruth S. Lieberman

✉ A.W. Stephan
andrew.stephan@nrl.navy.mil

1 U.S. Naval Research Laboratory, Washington, DC, USA

2 Space Sciences Laboratory, University of California, Berkeley, CA, USA

3 Virginia Polytechnic Institute and State University, Blacksburg, VA, USA

1 Introduction

The Ionospheric Connection Explorer (ICON) is a NASA mission that was launched in October 2019 to answer key questions about the response of the ionosphere to energy and momentum drivers in the troposphere and stratosphere below. ICON was placed into an approximately circular, 27-degree inclination orbit near 600 km altitude. The suite of remote sensing instruments is configured to view a similar volume of the ionosphere-thermosphere region, normally to the north of the orbit plane but occasionally using spacecraft maneuvers to aim the sensors toward the southern conjugate regions. The overarching mission goals, instruments, and measurement approaches are described by Immel et al. (2018) and references therein. Briefly summarized, ICON's science objectives are to understand: 1) the sources of strong ionospheric variability; 2) the transfer of energy and momentum from our atmosphere into space; and 3) how solar wind and magnetospheric effects modify the internally-driven atmosphere-space system.

The ICON EUV is a wide field, extreme ultraviolet (EUV) spectrograph that was designed to provide high-quality measurements of the daytime F-region ionosphere in support of the ICON science objectives (Sirk et al. 2017). Its specific requirements to meet the ICON science goals are to measure daytime ionospheric O^+ over an altitude range of 200-400 km with a vertical resolution of 20 km and 20% precision in the peak density, an in-track horizontal sampling of 500 km, and a temporal sampling of 60 seconds. The ICON EUV accomplishes this by continuously imaging one-dimensional vertical profiles of naturally occurring airglow emissions between 54-88 nm, covering the atmospheric limb between approximately 50-550 km tangent altitude, within a 12-second integration period. The approach used to infer ionospheric properties from these measurements, as described in Stephan et al. (2017), requires the simultaneous measurement of two of the brighter emissions of singly-ionized atomic oxygen (O^+) at 61.7 and 83.4 nm. Although the measurement most directly reflects the altitude profile of the O^+ ion species concentration, the ion concentration of the F-layer near its peak is typically on the order of 95% O^+. Thus, the measurement serves as a proxy for electron density in this layer as well as the key metric values for the height and density of the F-region ionospheric peak density, identified as hmF2 and NmF2 respectively.

The details regarding the history and implementation of the measurement and analysis approach for ICON have been described by Stephan (2016), Stephan et al. (2017), and references therein. In brief, the method is based on the process where (1) solar EUV photoionizes atomic oxygen in the lower thermosphere into an excited state, (2) the subsequent transition back to the ground state of O^+ produces photons in the 83.4 nm emission feature, and (3) these photons are then scattered and absorbed by ambient ionospheric O^+ ions. Thus the measured altitude profile of the emission depends on the characteristics of both the ionization source and the ionospheric scattering processes. Meanwhile, the emission near 61.7 nm derives from a transition between two excited states of O^+ and is therefore not easily modified by the ambient ionospheric oxygen ions that predominantly exist in the ground-state configuration. This emission thus represents a measure of just the thermosphere and the solar EUV photoionization source. Taken together these emissions are used to isolate ionospheric O^+ as the sole unknown and thereby infer the altitude profile of the density of the species.

This paper presents a review of the results from the ICON EUV obtained over the first year of the mission, the performance of the algorithm with respect to the ICON science requirements, changes and updates that have been made to the original algorithm in response to the as-measured data, and details on the results and caveats that are important for the scientific community to properly use and interpret these ionospheric data products. Additional details on the performance of the ICON EUV instrument can be found in Korpela

et al. (2022). A comprehensive analysis comparing and validating ICON EUV Level 2 data products to near-coincident ionospheric measurements made from GNSS radio-occultation, ionosondes, and incoherent scatter radar is presented by Wautelet et al. (2022).

2 Post-Launch Algorithm Modifications

Although the fundamental concept for the ICON EUV Level 2 algorithm has not changed from what was presented in Stephan et al. (2017), some modifications were implemented during the initial phases of data evaluation to improve not only the data quality but also to adjust to the computational reality of needing to process large volumes of data from the entirety of the mission in a timely manner using the finite computing resources shared by all ICON data product algorithms. In practice, these two factors are occasionally in conflict with each other which requires a delicate balancing of the approach. Here we note the key modifications that were implemented in versions leading up to Version 3 (v03) of these Level 2 data products.

First, it was observed that many of the original fits to the measured altitude profiles of the emissions were being controlled and driven to unrealistic solutions by the preponderance of measurements at the highest tangent altitudes. The sensor imaging pixels are defined by evenly-spaced viewing angles that translates to diminishing changes in tangent altitudes at the top of the altitude profile (tangent altitudes above about 500 km). Further compounding the issue was the fact that the airglow at the corresponding highest altitudes are regions with the dimmest airglow radiances, often effectively null as determined by the expected minimum measurable flux of 3.3 R (Sirk et al. 2017), resulting in an oversampled region of least relevance to the 61.7 and 83.4 nm airglow profiles. In addition, these higher-altitude look angles occasionally observed scattered light in the spectral signatures that resulted in larger background signatures that had to be removed from this dim airglow. In order to address this issue while maintaining a consistently-sized data field, the Level 2 analysis code was modified to select and process only 67 pixels of the full 108-pixel image; specifically pixels 16-82 (inclusive) corresponding to approximately 100-500 km tangent altitude. It is important to note that the bottom- and top-most six pixels of the detector image are outside the optical path and thus contain no relevant data. This tighter restriction ensures that the entirety of the relevant airglow profile is considered to enable the full range of expected ionospheres to be retrieved while cropping the lowest and highest tangent altitudes that are least important to the ionospheric profile.

Second, during evaluation of the algorithm performance early in the mission, it became apparent that it was possible to greatly enhance the speed of the calculation by breaking what was a complete and simultaneous two-color fitting into two separate and successive fitting processes. This was feasible because the primary purpose of the 61.7 nm emission was to provide a scaling term to the 83.4 nm photoionization source term. Since this is the only adjustable parameter in the 61.7 nm forward model, it could be directly and rapidly determined by first running a fit to this emission alone. With this common parameter then set in the 83.4 nm forward model, the subsequent iterative fit to the 83.4 nm emission to determine the ionospheric parameters could then be completed more rapidly because the number of free parameters was one fewer (requiring fewer evaluations of the 83.4 nm forward model) and the forward model for the 61.7 nm emission did not need to be evaluated in this step at all. This had the added benefit that the altitude regime under consideration for each emission feature could be independently set. While the full 67-pixel altitude profiles of the 61.7 nm emission are still reported in the Level 2 products, the model fit to the measured

61.7 nm emission was further restricted only to data with tangent altitudes below 300 km where the brightness of this emission is still higher than the minimum detectable threshold of the ICON EUV.

One particular concern that was examined was the potential for uncertainties in the shape of the modeled 61.7 nm emission profiles due to anticipated variations of the neutral atmosphere from true conditions. To evaluate this, the 61.7 nm forward model was adapted to check and adjust for an optimal shift of the data with respect to the model to optimize each fit. A simple scheme was devised to mimic an angular offset by moving the data up and down an integer number of pixels, effectively reassigning the viewing angle of each pixel to the one(s) above and below its original position in the image, to enable a rapid computation of the combined optimal vertical shift and scale factor to best fit each measured 61.7 nm emission profile. The end result is that the mean shift was determined to be on the order of less than a pixel. So while the resulting scale factor is applied to the forward model of the 83.4 nm emission to infer ionospheric characteristics, the vertical shift of any individual scan is not. As an additional test, an alternate extension of the code was devised to repeat a pre-flight algorithm test of the impact of varying neutral densities within the fitting process – however, such an adaptation was found to primarily alter the NmF2 factor in the same manner as the simpler single-scalar method. Although there is potential for such an approach to enable higher accuracy in ionospheric products, it was unnecessary in the scope of the ICON requirements for precision in NmF2 values, and computationally too expensive (more than doubling the typical processing time) to implement for bulk processing of the voluminous ICON EUV data set that nears one million individual measured altitude profiles in a year.

Third, it was demonstrated through extensive pre-flight testing that for a given input airglow profile the algorithm will naturally converge to the same fit and ionospheric solution regardless of the initial guess. However, the number of iterations required to achieve convergence will vary depending on how far away from the final result that initial guess starts. Thus, in the interest of computational efficiency, the algorithm was updated to use a standard starting point for the first profile (the first profile in the day, in the case of ICON where the data are combined and processed by day of year) and initialize each subsequent profile with the result from its predecessor. In the case where the orbit emerges from shadow, the first profile of the morning is still initialized with the last profile obtained near sunset from the previous orbit. In theory this will not affect the result; however, it has been found that the morning ionosphere prior to 10:00 local time (LT) is often insufficiently developed and results in an emission profile that is largely unperturbed by the low-density plasma. This, combined with the added uncertainties due to the higher solar zenith angles nearer to the terminator, makes the model output insensitive to adjustments in the fitting process and the algorithm often converges rapidly to a solution that can be influenced by the initial guess. For this reason, ICON EUV data collected prior to 08:00 LT (at the tangent location) are not processed, although some measurements even at this threshold remain mildly insensitive to ionospheric conditions. To examine this quantitatively, we have calculated the reduced χ^2 goodness-of-fit parameter (χ_v^2) using the formula (e.g. Bevington and Robinson 1992)

$$\chi_v^2 = \left(\frac{1}{\nu}\right)\left(\sum_{j=1}^{2n}\frac{[y_i - y(x_i)]^2}{\sigma_i^2}\right) \tag{1}$$

where y_i is the measured brightness, $y(x_i)$ represents the corresponding forward model value, and σ_i represents the statistical measurement uncertainties obtained for the EUV Level 1 data. The summation over $2n$ points describes the inclusion of n data points for
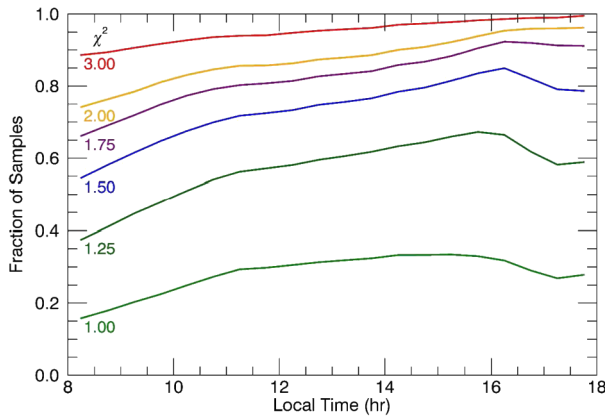
Fig. 1 A comparison of the fraction of samples resulting in a fit with a reduced χ^2 value of the fit less than the given value, versus the local time at the position of the measurement. Data are binned in half-hour increments, and each bin has approximately 50,000 samples with the exception of the two at the latest local times. The slightly poorer fits between the morning hours of 8-10 LT are largely a result of a poorly formed ionosphere, combined with the higher solar zenith angle of the measurements that also impacts the late afternoon local times

each altitude profile of the two colors (61.7 and 83.4 nm). The number of degrees of freedom, ν, is the number of degrees of freedom given by $(N - m)$, where $N = 2n$ and m is the number of parameters in the forward model used to fit the data. This parameter is informative in that a value close to 1 is ideal – smaller values are generally interpreted to be data where the assigned uncertainties are too large; values larger than 1 may indicate either assigned uncertainties that are too small or a true inability of the model to properly fit the data. Figure 1 shows the relationship between the local time of the measurement and the calculated χ^2_ν of the fit, with generally poorer quality fits in the early morning where this confluence of conditions exists. Higher reduced χ^2 near the afternoon (dusk) terminator after 1700 LT further reflects the uncertainties inherent in processing high solar zenith angle data, although the favorable ionospheric conditions during those hours greatly help to improve the quality of the fits.

The use of the prior result to initialize the next retrieval also set up a situation under certain conditions, particularly during the solar minimum period that many of the first year of ICON measurements were subject to, where the solution was near the limits of the model parameters, given by the range of allowed IG12 and Rz12 indices accepted by the IRI model, and the algorithm was unable to determine proper derivatives for identifying the next-step iteration. To resolve this, an additional check was implemented to ensure that if such a condition arose (on either the high or low end), that the initial guess of the next iteration was moved off the model limits to ensure proper functionality. This approach was successful, albeit at the expense of a modest impact to computational time.

3 Performance Evaluation

Based on the scientific goals of the ICON mission, the measurement requirement for the ICON EUV in the regions of interest, and most particularly within the latitudes surrounding the equatorial ionization anomaly, is to obtain the following: (1) hmF2 with 20 km vertical resolution, and (2) NmF2, with 20% precision, both over a 60 second sampling period. It is

Fig. 2 Cumulative distributions of the fraction of samples from the ICON EUV daytime ionosphere algorithm reporting uncertainties as described in the key. The performance of NmF2 is similar to mission simulations shown by Stephan et al. (2017). hmF2 is more greatly impacted by solar minimum conditions as the connection between O^+ and electron density becomes increasingly divergent, resulting in an insensitivity of the measurement method when hmF2 is lower than approximately 235 km
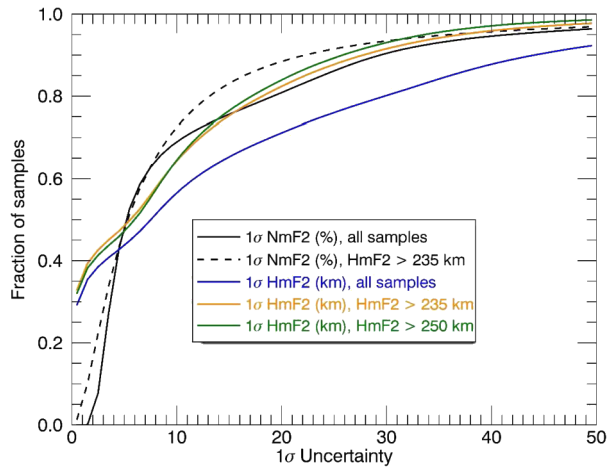
worthwhile to reiterate here that the primary ICON science goals are centered on identifying changes in ionospheric conditions, particularly in NmF2, so precision of NmF2 products is sufficient and necessary to address the main science goals of the mission. This is a particularly critical point in that accuracy of products depends on several additional factors, including the accuracy of the absolute radiometric calibration of both the 61.7 and 83.4 nm emissions that is determined largely by regular observations of the full moon, a method that has inherent limitations due to systematic uncertainties in the accuracy of our knowledge of both the solar flux and lunar albedo at EUV wavelengths. These combine to produce as much as a 13% systematic uncertainty in the reported brightness of each emission that could translate into systematic errors (biases) in NmF2 on the order of 60% or more. In practice, the current algorithm does not include any systematic uncertainties of the measured radiances in the fitting process or in the propagation of these uncertainties through to uncertainties in ionospheric products. These aspects are currently under evaluation but are beyond the scope and intent of the ICON goals, and of this manuscript. Any systematic uncertainties in the shape of the measured 83.4 nm profile that are not corrected by the routine flat-fielding measurements collected on-orbit (Sirk et al. 2017; Korpela et al. 2022) could also introduce significant errors in both hmF2 and NmF2.

For this work, we have examined v03 of the EUV Level 2.6 data products from the beginning of science operations in November 2019 through December 2020. In all, this represents 982,284 limb profiles that have been successfully processed to return ionospheric data products. We have not filtered any of the results other than what is specifically indicated in the discussion that follows. Although the measurement requirement is on a 60-second cadence, the native 12-second sampling has been maintained throughout the mission, and in this analysis, for several reasons. First, and most importantly, the in-flight, as-measured signal-to-noise has not dictated the need to co-add adjacent spectra to ensure sufficient precision in the data products. This is demonstrated in part by the data review that follows. Second, this allows data users to conduct a more detailed scrutiny of the finer sampling to assess the relevance of true ionospheric gradients in the samples as they relate to the measured samples. Third, this also facilitates the ability to assess and remove singular or small-batch samples that have out-of-family characteristics due to data anomalies and features that inevitably slip past the filters that are used in batch processing of the data. An example that highlights these latter two issues is presented in Sect. 5.
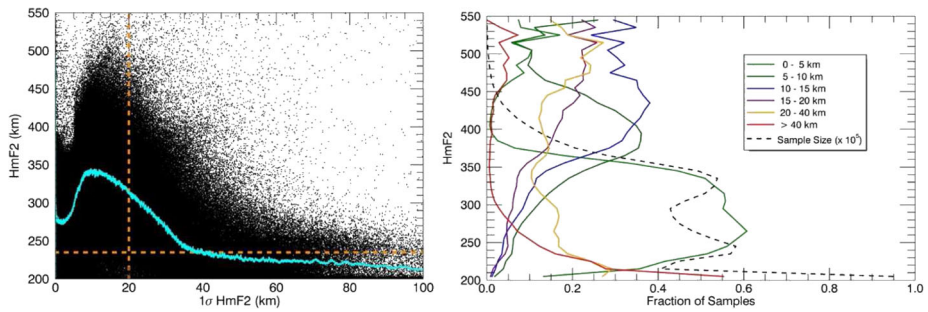
Fig. 3 Two representations of the retrieved uncertainties in hmF2 versus the retrieved hmF2 value itself from the ICON EUV data. On the left, the retrieved values are shown with respect to the required performance of better than 20 km represented by the vertical dashed line, along with a 1000-point boxcar-smoothed value of all the points shown (cyan line). The horizontal dashed line marks the 235 km altitude where the method begins to lose sensitivity due to the transition away from O^+ being the dominant ion in the ionosphere, as well as the movement of the scattering source closer to the peak in the production region in the lower thermosphere near 180 km. On the right, the fraction of samples at each reported hmF2 altitude that have reported uncertainties within the ranges indicated in the legend. The total number of samples within each altitude range (dashed line, scaled by 10^5) is also shown. The large number of samples with hmF2 near 200 km is a result of this being the lower threshold of allowed hmF2 values in the retrieval

Figure 2 shows a cumulative distributions of the fraction of total profiles with uncertainties less than a given value, analogous to the pre-flight tests presented by Stephan et al. (2017). In all, the realized performance is in reasonable agreement with these earlier simulations, indicating that the Level 1 EUV data are meeting performance expectations during this time. Statistically, more than 70% of the 12-second samples recover hmF2 with uncertainties less than 20 km. However, the distribution is different from our expectations in two ways. First, there is an apparent dual distribution of results, which are traceable to locations within and near the equatorial arcs versus those outside the arcs. Within the arcs, where the ionospheric peak is generally higher in density (NmF2) and altitude (hmF2), the algorithm returns hmF2 with reported uncertainties generally better than 5 km. This corresponds to more than 40% of the samples for ICON. Additionally, it has been found that as hmF2 drops below 250 km, the correlation between F-region O^+ and electrons become weaker and hmF2 is increasingly disconnected from the height where O^+ peaks in density. In these situations, the result is more dependent on the IRI-07 model capabilities to make this inferred connection. This correlation is shown more directly in Fig. 3, which includes the aggregate of all data points along with a (cyan-colored) curve showing the mean value of hmF2 that contributes to the corresponding uncertainty value. Based on an examination of results from the International Reference Ionosphere model (Bilitza and Reinisch 2008; Bilitza et al. 2017), it was found that as the ionosphere drops below this level the dominance of O^+ as the primary ion species wanes. Additionally, such an ionosphere may begin to exhibit less of a radiative transfer effect on the 83.4 nm photons (effectively becoming optically thin to O^+) as it moves closer to the peak of photoionization source in the lower thermosphere near 180 km. Redoing the distribution calculations with different altitude cut-offs shows similar distributions down to 235 km. Figure 2 shows this cut-off, as well as the 250 km cut-off for comparison. The analysis of NmF2 product is also shown in Fig. 2, where more than 68% of the 12-second samples return uncertainties of less than 10%, and nearly 78% of the samples report uncertainties less than 18%, the target for meeting ICON science goals. Although eliminating profiles with hmF2 lower than 235 km does have a minor effect on improving the reported uncertainties in NmF2, the effect is less than for hmF2. At these low altitudes,

the primary effect of the ionosphere is absorption of 83.4 nm photons, effectively dimming the brightness of the peak in the emission profile. This does not exclude the possibility of a systematic error in NmF2 for these low-hmF2 profiles in that the increased peak densities at low hmF2 values will still have some impact on the emission brightness, albeit not in full proportion to the true peak densities in the O^+ profile. Based on inspection of the data in Fig. 3, including both the larger-uncertainty tail and the distribution of uncertainties near 10 km, this threshold for creating a warning of a possible systematic uncertainty in the EUV Level 2 data products has been set at 235 km.

A related and important consideration for the ICON EUV method prior to launch of the ICON mission centered around the performance impact caused by launch delays that pushed the start of the mission into the deepest part of solar minimum. The combination of a lower solar EUV flux and the contraction of the terrestrial thermosphere would result in lower source emission, and the corresponding lower ionospheric densities would result in less of a scattering effect that would hinder the detectability and determination of the O^+ profile. Extensive pre-flight simulations were conducted to demonstrate that the measurement and retrieval would still be effective under these conditions. Data from the Limb-imaging Ionospheric and Thermospheric EUV Spectrograph (LITES) that began collecting EUV airglow data from the International Space Station in early 2017, when F10 was already well into solar minimum, showed direct evidence that the method could still be used to detect ionospheric signatures at least in the equatorial arcs (Stephan et al. 2019) – the region of highest interest to the objectives of the ICON science goals.

Additional consideration was given to the fact that the forward model derived from determinations of the excitation efficiency, or g-factor, under the assumption of F10.7 $\geq$ 75, which would require scaling or extrapolation to the realized F10.7 flux values that reached a minimum of near 60 sfu in late 2019 (https://www.spaceweather.gc.ca/forecast-prevision/solar-solaire/solarflux/sx-en.php). Several comparisons were made between results that used the g-factors derived with F10.7 of 75 sfu, scaled as part of the fitting process to data obtained at lower F10.7 values, to tests completed with a direct computation of g-factors using both the Hinteregger solar EUV model (Hinteregger et al. 1981) and an updated solar EUV flux model (Lean et al. 2011). These tests of both simulated and early-orbit ICON EUV data found nearly identical ionospheric products despite the expectedly different resulting emission rate scalars necessary for each. These tests confirmed the pre-flight determination that the method and inversion approach would remain valid through lower solar activity, largely through the use of a scalar on the volume emission rate that corrects for the limitations of the extrapolation under extreme solar minimum. It also exemplifies the application of the emission rate scalar to offset unknowns in the solar EUV flux. This scalar will be discussed further in the next section.

Figure 4 shows time history of the retrieved uncertainties in hmF2, identical to those shown in Fig. 2, from the beginning of science operations for the ICON EUV instrument on 18 November 2019, compiled through the end of 2020. The brief outage between day 95-100 in this plot was caused by the spacecraft entering safe mode following an anomaly with the star tracker. A 1000-point boxcar-smoothed average of all the data is shown (cyan), showing the long-term trends in the quality of the data returned by the Level 2 EUV retrieval algorithm. The orbital parameters result in a phasing between sampling of local time and latitude that creates a 42-day repetition of the measurement that is seen here, with higher reported uncertainties when the daytime measurements are mostly constrained to the northern-most latitudes away from the equatorial arcs, and lower overall uncertainties when the measurements fully cross through the equatorial latitudes where the higher-interest and higher-quality data are obtained. Figure 5 shows a similar time history of percentage uncertainties in retrieved NmF2. The orbital phasing seen in hmF2 is represented in these data as
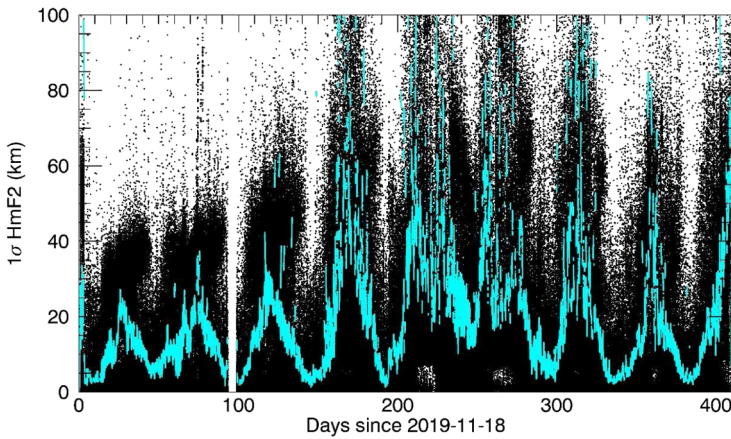
Fig. 4 Retrieved uncertainties in hmF2, identical to those shown in Fig. 3, here represented as a function of time from the beginning of science operations for the ICON EUV instrument on 18 November 2019, compiled through the end of 2020, along with a 1000-point boxcar-smoothed average of all the data (cyan line). The 42-day periodicity in local time and latitude sampling of the orbit, and subsequent phasing of the orbital solar beta angle, results in the oscillations with higher reported uncertainties when the daytime measurements are mostly constrained to the northern-most latitudes, and lower overall uncertainties when the measurements fully cross through the equatorial latitudes
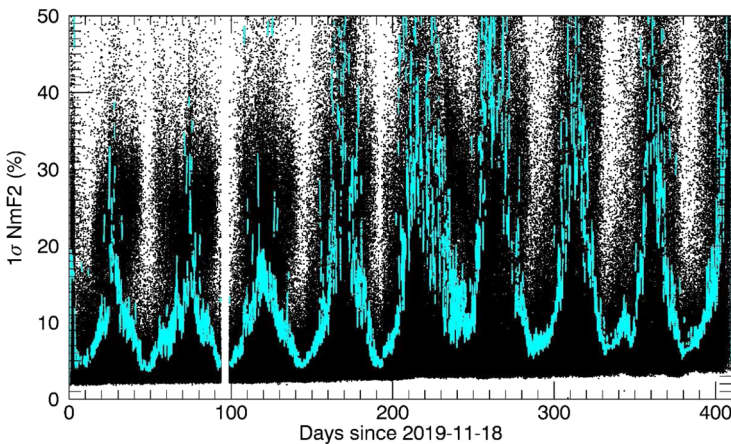

Fig. 5 Uncertainties in retrieved NmF2, represented as a function of time from the beginning of science operations for the ICON EUV instrument on 18 November 2019, compiled through the end of 2020, along with a 1000-point boxcar-smoothed average of all the data (cyan line). The orbital phasing present in hmF2 as shown in Fig. 4 is represented in these data as well

well. Figure 6 shows the reduced χ^2 value of the fit to the combined 61.7 and 83.4 nm data as first presented in Fig. 1, but here showing temporal patterns over the mission. In general, the forward model is able to obtain good fits to the measured data, with the majority of the fits achieving $0.5 < \chi^2_\nu < 2.0$. No evidence is seen for any periodicity that was seen in the ionospheric parameter uncertainties. This confirms that the model is generally able to achieve good fits to the measured profiles, and that higher uncertainties are created by the conditions that are being measured. Some periods do show times where many of the fits are
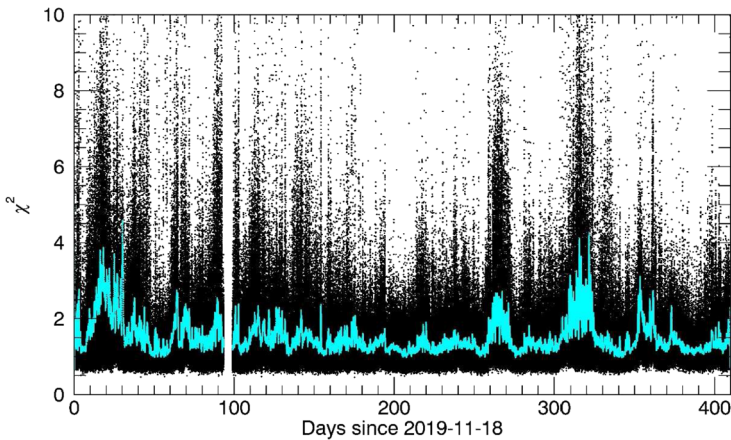
Fig. 6 Reduced χ^2 value of the fit to the combined 61.7 and 83.4 nm data represented as a function of time from the beginning of science operations for the ICON EUV instrument on 18 November 2019, along with a 1000-point boxcar-smoothed average of all the data (cyan line). In general, the forward model is able to obtain good fits to the measured data, with the majority of the data achieving values between 0.5 and 2.0
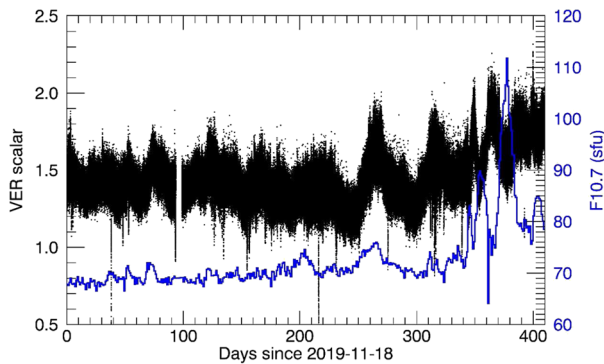

Fig. 7 Time history of the inferred volume emission rate (VER) scalar applied to the forward model to match the measured ICON EUV 61.7 nm emission peak radiance. Also shown is the solar F10.7 cm flux, in solar flux units (sfu) used within the algorithm primarily to condition the NRLMSIS thermospheric model. The anomalously low F10.7 value of 64 sfu near day 360 in this sequence is an apparently erroneous data point that was corrected to the proper value of 80.2 sfu in the final processing

not as good, warranting closer inspection, although the number of samples is generally not overwhelming – these outliers are overemphasized when averaging data, as was done here to demonstrate the trend in temporal history over this first year of the mission.

Figure 7 shows the history of scalars applied to the volume emission rate of the 61.7 nm emission to match the measured peak radiance. This scalar is designed to provide an adjustment for any combination of systematic biases in the measurement, including absolute calibration errors in the Level 1 radiance products, solar EUV and thermospheric density changes not captured in the empirical NRLMSIS model, and uncertainties in the forward model that include but are not limited to the specification of the g-factors that define the excitation rate or photoabsorption cross sections (e.g. Stephan et al. 2012; Stephan 2016). Each of these factors will manifest as a slightly different long- and short-term impact on

this scalar. It is noted here that any differential systematic calibration error between 83.4 nm and 61.7 nm emissions is not resolved by this scalar and will manifest as a systematic offset in NmF2, which will affect the accuracy of the NmF2 products. For example, if the ICON EUV sensitivity is underestimated at 61.7 nm and/or overestimated at 83.4 nm, the retrieved NmF2 will be systematically low. However, this has not been found to affect the precision that is the target of the ICON science measurements, and would only become important if the relative calibration accuracy between the two colors is variable and uncorrected by the routine radiometric calibration and flat-field measurements that are obtained and applied to the data. Significant changes in this regard would also potentially be observable in the model intensity scalars that are retrieved, although there is no evidence of this to date.

There are several interesting trends in this scale factor worth noting. The first observation is that there exists a lower threshold of about 1.4 that suggests a systematic error in either the calibration of the EUV sensor or the forward model, and likely both. A relatively uniform value is found at the beginning of the data collection in November 2019 when F10.7 (shown in blue in Fig. 7) is steady and low, with some minor oscillations that phase closely with the 42-day orbit sampling periodicity that suggest a very minor connection to patterns in the solar zenith angle, latitude, and local time of the measurements. As F10.7 slowly begins to increase through 2020, the required scalar shows an overall positive correlation ($r = 0.21$). This is most likely caused by an underestimation of atomic oxygen densities in the NRLM-SIS model for F10.7 values less than about 100 sfu (Emmert et al. 2008; Meier et al. 2015) meaning that the volume production rate is correspondingly underestimated during these times. A small negative correlation between F10.7 and the scalar value also appears to occur and may be related to a correspondingly small systematic error in the radiometric calibration of the Level 1 EUV data product, although a more detailed study is necessary to confirm that hypothesis. The second key observation is found by examining the last few months of 2020 when solar activity is greatly increased. While the overall trend still shows a visible positive correlation with F10.7, short-term variations show a strong negative correlation ($r = -0.48$). This is believed to be a result of the fact that in order to facilitate near-real-time inversions of the data, the 81-day F10.7 value is not used to drive the thermospheric NRLMSIS model – instead, the daily F10.7 value is used, under the expectation that this will be corrected through the use of the scalar in the model. In this case, the temporary drop in F10.7 does not capture the overarching higher level of activity that would be addressed through the 81-day F10.7 value, resulting in an increase in the required scalar during these times. Future data reprocessing will use the archived 81-day average to further evaluate this aspect of the inversion algorithm, although this is a low-priority for the ICON computing resources at this time given the success of the current approach. These results are an encouraging demonstration that the algorithm is adapting and correcting for the true underlying thermospheric state during these changing conditions, as expected and intended.

4 Data Interpretation and Usage

It is always encouraged that, prior to beginning any study, users of the ICON data products make contact with the key points of contact on the team, as laid out in the notes contained within the distributed NetCDF files. This ensures that any nuances that may be relevant to the interpretation and application of the data products are reviewed and understood. Here we highlight a few of the key aspects that we expect will be most relevant to all users of the ICON EUV Level 2 data products.

First, the ionospheric data products are always geolocated to the position where the line-of-sight tangent altitude is 300 km. This ensures consistency across the EUV measurements for comparisons, but it is important to note that because of the nature of the radiation transfer problem the true ionospheric location may be somewhat different in reality than this reference value reflects. It is plausible for users to recalculate positions based on the reported hmF2 values, but generally the difference is expected to be small. For example, a 50 km difference in hmF2 (e.g. 300 ± 50 km) corresponds to an approximate 1.5 degree change in latitude, closer or farther to the ICON spacecraft for higher and lower hmF2 values, respectively. Changes in geographic longitude are generally insignificant with respect to the 12-degree horizontal EUV field of regard. Any remapping, however, may require a new computation of both the corresponding location in geomagnetic latitude and longitude that will have different dependencies from geographic coordinates. Consideration should also be given to the fact that the 12-degree horizontal field maps to a horizontal extent of about 350 km at the 300 km tangent altitude location, and the motion of the spacecraft during the 12-second integration covers nearly 90 km (and 0.75-degrees of longitude) over which data are integrated. All geolocation positions reported with the ICON EUV data, however, are determined specifically in the middle of the 12-second integration, and the center of the horizontal and vertical extents of each image point at that time.

Second, the measurement uses a two-color approach to resolve otherwise inherent ambiguities between changes in the thermospheric source of 83.4 nm photons and the ionospheric scattering effects. This does not mean, however, that all systematic biases have been removed. As previously highlighted, while ICON EUV maintains the *precision* of its NmF2 products to within the desired 20% as shown in Fig. 2, it cannot guarantee the *accuracy* of these products. This is because there are significant uncertainties in the radiometric calibration that relies on scans of the EUV field of regard across the full moon (Sirk et al. 2017). While the calibration approach allows corrections for temporal changes in sensor responsivity over the span of days and months, it cannot provide the accuracy of absolute calibration that would be needed to meet any accuracy requirement for retrieved products. In addition to the absolute calibration of each wavelength, the NmF2 product also has a dependence on the relative calibration between the two measured colors as well. Simulations have found that the NmF2 is highly sensitive to accuracy of the EUV sensor calibration, where even a 5% error in absolute responsivity results in up to 20% errors in absolute NmF2 (Stephan 2016). Validation comparisons of these results with ground-truth reference measurements are presented by Wautelet et al. (2022).

Finally, balancing the performance speed with data quality means that some profiles may show inconsistent results – best practices for usage of specific singular profiles would dictate that although the data are reported at their native 12-second cadence, that a sequence of at least five profiles, equivalent to the ICON EUV measurement requirement of 500 km or 60-second sampling, be evaluated to ensure consistency through the timespan. This aspect is discussed in more detail in the next section.

5 Example of Results

Two different sets of results are presented here to demonstrate more specific ways in which the ICON EUV data can be applied in support of scientific studies, as well as demonstrate potential caveats that should be considered prior to interpretation. The first example represents longer term data aggregation to understand regional and global ionospheric patterns
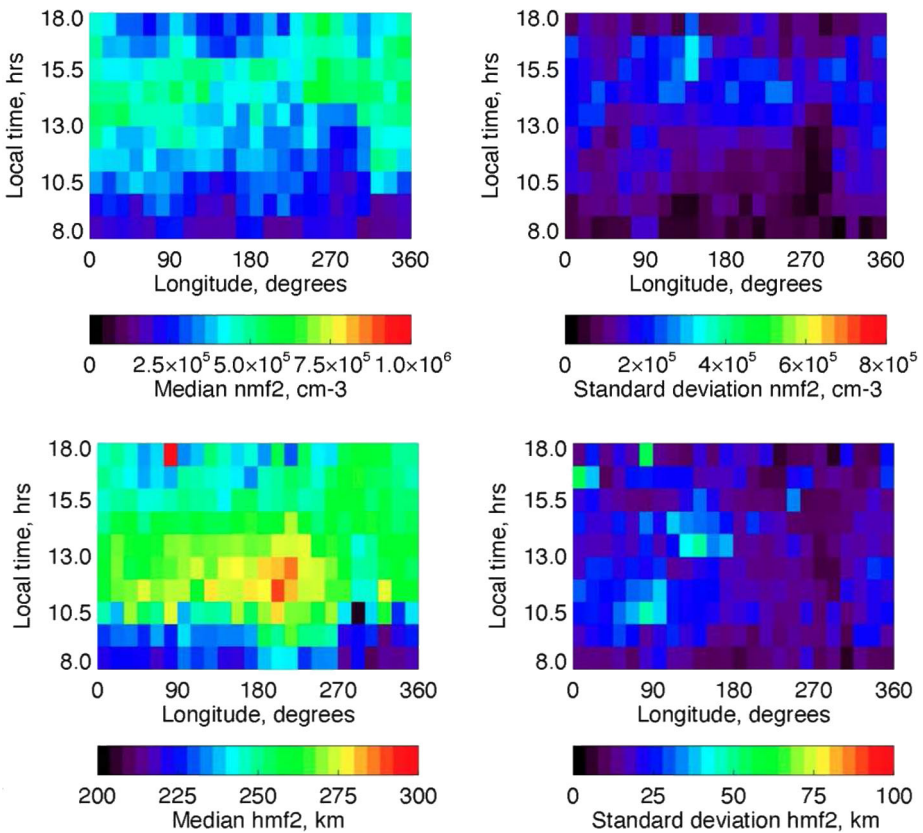
Fig. 8 Local time – longitude maps of aggregated ICON EUV hmF2 and NmF2 data collected between magnetic latitudes of 15-30 degrees, compiled over one orbit precession cycle starting on 13 March 2020. Only data reporting a good quality flag (0 or 1) are kept and data with a poor quality flag (2) are excluded. Left-side plots show median values and right-side plots show the corresponding 1σ standard deviations

that are the targets of the ICON science objectives, while the second demonstrates a higher-fidelity review of a single orbit pass through low latitudes that may be undertaken to support a targeted measurement campaign. However, no formal scientific conclusions are intended or presented as a part of this limited data review.

Figure 8 shows a mapping of longitude and local time patterns in ionospheric hmF2 and NmF2 aggregated over one orbit precession cycle of the ICON observatory. These measurements were collected between 13 March 2020 (day of year 73) and end on 24 April 2020 (day of year 115), near the vernal equinox. Only data reporting a good quality flag (warning level 0 or 1) are kept and data with a poor quality flag (warning level 2) are excluded. The primary cause of a level 2 warning that still returns an ionospheric result in the Level 2 data products is $\chi^2 > 3$ (see also Stephan et al. 2017, as well as corresponding notes contained in the ICON EUV Level 2 data products for additional detail). The figures include all such measurements made between 15-30 degrees of geomagnetic latitude, covering the region of the northern arc of the equatorial ionization anomaly. The 1-sigma standard deviation in these values is also shown. What this map shows is the general increase in NmF2 through the morning into the afternoon hours, with a wave-4 signature particularly visible in the 13-16

Fig. 9 A map of the orbit track of ICON between 0825-0835 UT on 23 November 2019 (blue diamonds), and the location of the tangent point at altitude of 300 km (black asterisks), along with the location of the geomagnetic equator for this region (orange line). The orbit passes through local times of 1412 to 1622 as it moves from west to east, and south to north for this segment
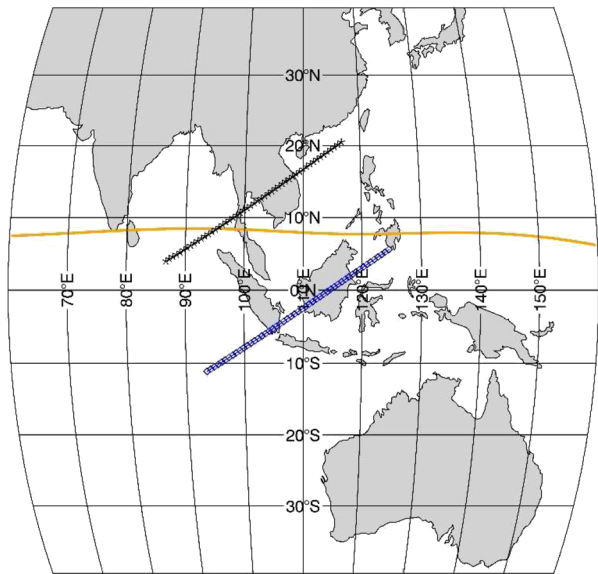
LT range. The differences exceed the measured standard deviation of the samples, and thus can be viewed as a demonstration of the natural, persistent geophysical ionospheric pattern seen during this time. The most striking feature in the map of hmF2 is the uniquely high value near local noon in the longitude sector between 180-225 degrees. While it is difficult to fully ascribe a cause without further examination of the evidence, it is perhaps noteworthy that this sector is where the geomagnetic equator nearly coincides with the geographic equator, resulting in a corresponding intersection between the sub-solar point for this region and the boundary region in geomagnetic coordinates that is used to create this map.

A second example, highlighting a specific measurement sequence, has been chosen to further demonstrate the applicability and potential caveats of the ICON EUV data. This sample was taken between 08:25-08:35 UT on 23 November 2019, near the start of routine science operations for the ICON EUV. A map of both the location of the ICON observatory and the 300-km tangent altitude location of the ICON EUV field of view is shown in Fig. 9. This particular segment was chosen to highlight some particular aspects of the EUV measurements, specifically (1) the typical extent of the region of space that is sampled by the airglow imager, (2) the effect that the combination of changing latitude and local time of the measurement across a pass of a low-inclination orbit may have on sampling, co-adding, and interpreting and comparing specific data samples, and (3) the impact that systematic errors in the sampled Level 1 data can have on the retrieved ionospheric products.

Figure 10 shows the sequence of hmF2 and NmF2 values returned by the EUV Level 2 algorithm for this sequence of measurements. The change in hmF2 suggests a singular peak in electron density very near the magnetic equator. Additionally, the sub-solar location for this time of year is in the southern hemisphere, moving the location of the expected peak of solar-produced plasma production closer to the spacecraft than this figure represents. It is notable that there is the lack of a second peak as the spacecraft and the corresponding tangent-point latitudes move north across the magnetic equator, and inspection of the data also shows no separate peak to the south, earlier in this orbit. However, the spacecraft is also rapidly moving in local time and crosses the terminator shortly thereafter, where the EUV measurements no longer apply. So while there is no evidence of a second peak up until this

Fig. 10 hmF2 and NmF2 values returned by the EUV retrieval for the orbit segment shown in Fig. 9. Note that the propagated statistical errors result in uncertainties for hmF2 that are on the order of 1 km for much of this pass
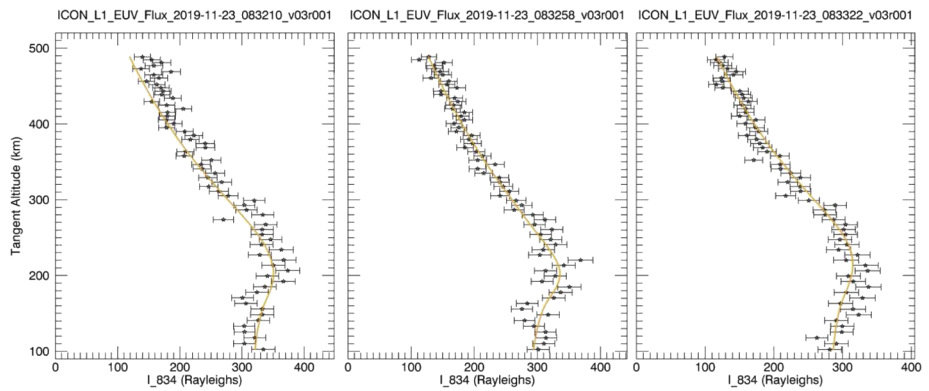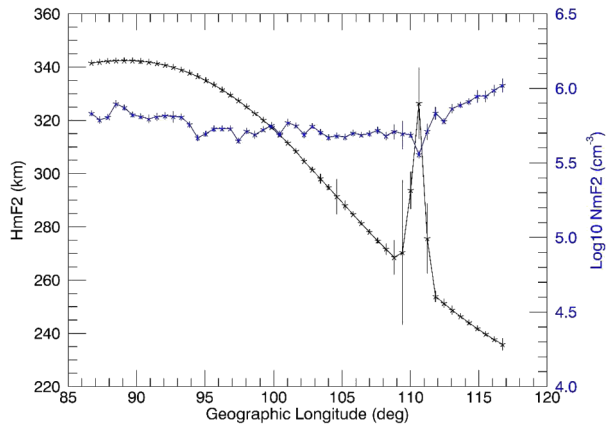
Fig. 11 Sequence of fits to the 83.4 nm emission. The middle image corresponds to the anomalously high hmF2 value seen in Fig. 10. To the left is the profile 48 seconds (4 image samples) prior, and to the right is the profile from 24 seconds (2 image samples) after, when hmF2 values are in family with the sequence of results

threshold is crossed, the sampling from such an orbit cannot explicitly address this question on an isolated case-study basis. However, these results do suggest that the plasma fountain has not impacted the overarching ionospheric plasma distribution at this time.

The second interesting aspect of this figure is the uncharacteristic and unrealistic spike in hmF2 near longitude of 110 degrees in Fig. 10. In the data shown here, all of the fits return reasonable values and do not generate any warning flags that would suggest the data are not trustworthy, other than a notification that the measurements are taken under low F10.7. Reported hmF2 values are above our warning threshold of 235 km discussed earlier in this presentation. So while this represents a real and valid result of the retrieval, its source does not appear to be a real geophysical change. Figure 11 provides a snapshot of samples in the reported 83.4 nm radiance profile obtained by the ICON EUV during this pass. Three samples taken through this sequence are shown: the center panel shows the measured altitude profile of the 83.4 nm emission and the fit that corresponds to the anomalously high hmF2 value seen in Fig. 10, the left panel shows the measured altitude profile taken 48 seconds (four image samples) prior, and the right panel shows the measured altitude profile from 24 seconds (two image samples) after. The latter two represent profiles when hmF2 values ap-

pear to be in family with the full sequence of values. What these panels show is perturbations in the measured radiance below 200 km that takes on the appearance of real structure in the measured flux that subsequently drives the algorithm to an alternate solution. This is almost certainly a result of the automated processing software required for handling the large volume of EUV data, that cannot possibly capture all of the nuances of noise, background and scattered light sources, and other irregularly occurring detector phenomena that might appear. It is important to reiterate that all of these profiles are identified as reasonable – the fits are good and no other warnings are in place to capture this type of effect in the Level 2 data products. Even the reported uncertainties inside the spike, while larger than those reported for the adjacent samples, are not sufficient to capture the systematic error here because the random uncertainties are relatively similar across all the profiles. Given the absence of an ionospheric cause, it may be that a small short-duration change in the characteristic flat-field, or even an unknown emission source at higher altitude (e.g. solar 83.4 nm) may be contributing to the 83.4 nm emission profile that the inversion is particularly sensitive to. Also noteworthy is the counter-effect on NmF2 which appears to be somewhat uncharacteristically smaller for the measurement that returns the most anomalous hmF2 value, compared to adjacent values. However, the variability of NmF2 which generally is highly sensitive to errors in the radiance, shows point-to-point variation that may indicate real changes in the relative ionospheric structure, although here is an important reason to consider the ICON science requirements that expect no better than 60-second sampling, equivalent to five measurement points, when assessing the significance of rapid changes in the measured products. Although we have sufficient signal-to-noise to maintain the 12-second cadence in the data products, analysis particularly involving NmF2 would likely benefit from considering averages or smoothing over five samples (60-second) to mitigate the sensitivity to such small statistical changes in the measured radiance.

6 Summary

We have examined more than a year of daytime ionospheric products obtained from the ICON EUV spectrometer and find that in the geographic regions of interest the quality of the data is meeting the performance requirements to address the ICON science goals, with 1σ uncertainties in hmF2 better than 20 km, and NmF2 better than 20% in precision. When filtering out measurements taken near the physical limitations of the measurement approach, specifically when hmF2 falls below 235 km, the performance falls in line with performance expectations from the mission pre-flight simulations. This has been maintained despite low solar activity due to the resiliency of the Level 2 algorithm that uses the paired 61.7 nm /83.4 nm emissions to directly compensate for such conditions. The assessment of additional systematic uncertainties in the absolute radiances of the measured profiles is necessary to further improve the accuracy of the retrieved NmF2, which can be completed in part using comparisons to ground-truth ionospheric measurements. This aspect, however, is beyond the requirements of the ICON mission for precision in NmF2 to identify ionospheric changes over a 500 km great circle (60-second integration). Active evaluations have allowed tradeoffs in algorithm speed versus performance to be made, to ensure the highest quality product is created with reasonable burden on computational resources. Autonomous processing does potentially create isolated cases where retrieved products could be driven by measurement artifacts that slip through the best processing methods available, requiring diligence from users of the data to ensure all aspects of data quality are evaluated.

Data Availability This analysis used version 03 of the Level 2.6 ICON-EUV data which are available from the ICON website (https://icon.ssl.berkeley.edu/Data) and NASA's Space Physics Data Facility (https://cdaweb.gsfc.nasa.gov/pub/data/icon/).

Declarations

Competing Interests The authors have no competing interests to declare that are relevant to the content of this article.

References

Bevington PR, Robinson KR (1992) Data reduction and error analysis for the physical sciences. McGraw-Hill Inc., New York

Bilitza D, Reinisch BW (2008) International reference ionosphere 2007: improvements and new parameters. Adv Space Res 42:599–609. https://doi.org/10.1016/j.asr.2007.07.048

Bilitza D, Altadill D, Truhlik V, Shubin V, Galkin I, Reinisch B, Huang X (2017) International reference ionosphere 2016: from ionospheric climate to real-time weather predictions. Space Weather 15:418–429. https://doi.org/10.1002/2016SW001593

Emmert JT, Picone JM, Meier RR (2008) Thermospheric global average density trends, 1967–2007, derived from orbits of 5000 near-earth objects. Geophys Res Lett 35(5):L05101. https://doi.org/10.1029/2007gl032809

Hinteregger HE, Fukui K, Gilson BR (1981) Observational, reference and model data on solar EUV from measurements on AE-E. Geophys Res Lett 8:1147–1150. https://doi.org/10.1029/GL008i011p01147

Immel TJ, England SL, Mende SB, Heelis RA, Englert CR, Edelstein J et al (2018) The ionospheric connection explorer mission: mission goals and design. Space Sci Rev 214(1):13. https://doi.org/10.1007/s11214-017-0449-2

Korpela EJ, Sirk MM, Edelstein J, McPhate JB, Tuminello RM, Stephan AW et al (2022, submitted) In-flight performance of the ICON EUV spectrograph. Space Sci Rev

Lean JL, Woods TN, Eparvier FG, Meier RR, Strickland DJ, Correira JT, Evans JS (2011) Solar extreme ultraviolet irradiance: present, past, and future. J Geophys Res 116:A01102. https://doi.org/10.1029/2010JA015901

Meier RR et al (2015) Remote sensing of Earth's limb by TIMED/GUVI: retrieval of thermospheric composition and temperature. Earth Space Sci 2:1–37. https://doi.org/10.1002/2014EA000035

Sirk MM, Korpela EJ, Ishikawa Y, Edelstein J, Wishnow EH, Smith C et al (2017) Design and performance of the ICON EUV spectrograph. Space Sci Rev 212:631–643. https://doi.org/10.1007/s11214-017-0384-2

Stephan AW, Finn SC, Cook TA, Geddes G, Chakrabarti S, Budzien SA (2019) Imaging of the daytime ionospheric equatorial arcs with extreme and far ultraviolet airglow. J Geophys Res Space Phys 124:6074–6086. https://doi.org/10.1029/2019JA026624

Stephan AW, Korpela EJ, Sirk MM, England SL, Immel TJ (2017) Daytime ionosphere retrieval algorithm for the Ionospheric Connection Explorer (ICON). Space Sci Rev 212:645. https://doi.org/10.1007/s11214-017-0385-1

Stephan AW (2016) Advances in remote sensing of the daytime ionosphere with EUV airglow. J Geophys Res Space Phys 121:9284–9292. https://doi.org/10.1002/2016JA022629

Stephan AW, Picone JM, Budzien SA, Bishop RL, Christensen AB, Hecht JH (2012) Measurement and application of the O II 61.7 nm dayglow. J Geophys Res 117:A01316. https://doi.org/10.1029/2011JA016897

Wautelet G, Hubert B, Gérard J-C, Immel TJ, Sirk MM, Korpela EJ et al (2022) Comparison of ICON-EUV F-peak characteristic parameters with external data sources. Space Sci Rev 218:62. https://doi.org/10.1007/s11214-022-00930-2

Publisher's Note Springer Nature remains neutral with regard to jurisdictional claims in published maps and institutional affiliations.